The Role of S100P in the Invasion of Pancreatic Cancer Cells Is Mediated through Cytoskeletal Changes and Regulation of Cathepsin D

Hannah J. Whiteman,[1] Mark E. Weeks,[1] Sally E. Dowen,[1] Sayka Barry,[1] John F. Timms,[2] Nicholas R. Lemoine,[1] and Tatjana Crnogorac-Jurcevic[1]

[1]Centre for Molecular Oncology, Institute of Cancer, Barts and The London School of Medicine and Dentistry, Queen Mary University of London; [2]Cancer Proteomics Laboratory, Institute for Women's Health, University College London, London, United Kingdom

Abstract

Up-regulation of S100P, a member of the S100 calcium-binding protein family, is an early molecular event in the development of pancreatic cancer and it is expressed at high levels in both precursor lesions and invasive cancer. To gain more insight into the molecular mechanisms underlying the functional roles of this protein, we stably overexpressed S100P in the Panc1 pancreatic cancer cell line and identified the consequent changes in global protein expression by two-dimensional difference in-gel electrophoresis. The observed changes in target proteins were confirmed by Western blot analysis and immunofluorescence, whereas their functional effect was investigated using motility and invasion assays. In this study, we have shown that overexpression of S100P led to changes in the expression levels of several cytoskeletal proteins, including cytokeratins 8, 18, and 19. We have also shown disorganization of the actin cytoskeleton network and changes in the phosphorylation status of the actin regulatory protein cofilin. Additionally, we have shown that overexpression of S100P leads to increased expression of another early pancreatic cancer marker, S100A6, as well as the aspartic protease cathepsin D, both of which are involved in cellular invasion. Functional studies showed that the increased invasive potential of S100P-overexpressing cells was at least partially due to the increase in cathepsin D expression. In summary, our data suggest that these changes could contribute to the metastatic spread of pancreatic cancer and may explain the devastating prognosis of this disease. [Cancer Res 2007;67(18):8633–42]

Introduction

Pancreatic ductal adenocarcinoma (PDAC) is the fourth most common cause of cancer-related deaths in the industrialized world, accounting for >32,000 deaths each year in the United States (1). The disease has a dismal prognosis and a 5-year survival rate of <5% because it usually remains undiagnosed until a late stage (2, 3).

S100P is a member of the S100 family of EF-hand calcium-binding proteins (4). It was first purified from placenta (hence the "P"; ref. 5) and has subsequently been detected in several types of cancer (6), including breast (7), colon (8), and prostate (9). Increased levels of S100P expression have also been found to correlate with poor survival in breast (10) and lung cancer (11).

In PDAC, several members of the S100 calcium-binding protein family are up-regulated (12). Two members of this family, S100P and S100A6, show a steady increase in expression from pancreatic intraepithelial neoplasia (PanIN) precursor lesions to PDAC, suggesting a critical role for these proteins in disease progression (13–16).

Although the mode of action of S100P is largely unknown, several recent studies have examined its role in pancreatic cancer cells (14, 17–19). Work by Arumugam et al. (18) showed that S100P regulates proliferation, migration, and survival of pancreatic cancer cells, with decreased metastatic potential *in vivo* following S100P knockdown.

To investigate the molecular mechanisms of S100P activity, we used two-dimensional difference in-gel electrophoresis (2D-DIGE) to conduct a global analysis of proteins regulated following its overexpression in Panc1 cells, which have negligible endogenous levels of S100P. An alternative cell line with low S100P expression, HPDE, although usually referred to as a normal ductal cell line, is immortalized with human papillomavirus E6/E7 (20) and hence has abrogated Rb1 and p53 pathways. Moreover, during its establishment, it acquired resistance to G418, the selection agent required for our S100P-overexpressing stable cell lines, and was therefore unsuitable for our study. 2D-DIGE allows simultaneous analysis of several samples on the same gel after covalent labeling of control and experimental samples with different fluorescent tags. By alleviating the problems of gel-to-gel variation, the 2D-DIGE strategy provides improved accuracy in quantifying protein differences between samples (21–23).

Using this system, we identified several S100P-dependent changes in protein expression, which were confirmed using Western blotting and immunofluorescence. In addition, motility and invasion assays have been conducted to investigate how these changes contribute to S100P-dependent tumor progression.

Materials and Methods

Cell lines and plasmids. Panc1 cells (24) were obtained from Cancer Research UK Cell Services and cultured in E4 medium (Cancer Research UK Media Production) supplemented with 10% heat-inactivated FCS (Life Technologies, Invitrogen). The pcDNA3.1/S100P-V5-His and pGEX-S100P constructs used in this study have been described previously (14).

Establishment of S100P-overexpressing stable cell lines. Panc1 cells were seeded at 2×10^6 per 10-cm-diameter plate and transfected using FuGENE6 (Roche Diagnostics) in a 3:1 ratio, with pcDNA3.1/S100P-V5-His or pcDNA3.1/V5-His. Stable cell lines were established following selection with 1.2 mg/mL G418 (Life Technologies).

cDNA synthesis and reverse transcription-PCR. cDNA was synthesized from 1 μg total RNA using the MultiScribe Reverse Transcription kit (Applied Biosystems) and oligo(dT) primers. Reverse transcription-PCR

Note: Supplementary data for this article are available at Cancer Research Online (http://cancerres.aacrjournals.org/).

H.J. Whiteman and M.E. Weeks contributed equally to this work.

Requests for reprints: Tatjana Crnogorac-Jurcevic, Centre for Molecular Oncology, Institute of Cancer, Barts and The London School of Medicine and Dentistry, Queen Mary University of London, Charterhouse Square, London EC1M 6BQ, United Kingdom. Phone: 44-20-7014-0427; Fax: 44-20-7014-0431; E-mail: T.C.Jurcevic@qmul.ac.uk.

doi:10.1158/0008-5472.CAN-07-0545

(RT-PCR) was done using the following primers: S100P, 5′-TGCAGAGTGGAAAAGACAAGGAT-3′ (forward) and 5′-CCACCTGGGCATCTCCATT-3′ (reverse); control 18S rRNA, 5′-CGCCGCTAGAGGTGAAATTC-3′ (forward) and 5′-CATTCTTGGCAAATGCTTTCG-3′ (reverse).

Western blot analysis. Cells were lysed in either NP40 lysis buffer [1% NP40, 50 mmol/L Tris (pH 7.4), 150 mmol/L NaCl] with Complete Protease Inhibitor Cocktail tablets (Roche Diagnostics) or Triton X-100 lysis buffer [1% Triton X-100, 50 mmol/L TBS (pH 7.4), 10 mmol/L EDTA with protease inhibitors]. Lysates were centrifuged and the insoluble material was solubilized by the addition of loading buffer [45 mmol/L Tris (pH 6.8), 10% glycerol, 1% SDS, 50 mmol/L DTT, 0.01% bromphenol blue] to the cell debris followed by treatment with 2 μL benzonase (Merck) per 50 μL sample for 1 h at room temperature. For SDS-PAGE, 10 to 20 μg of protein, diluted in loading buffer (see above), were separated on a NuPAGE 4% to 12% Bis-Tris gel (Invitrogen) and transferred onto polyvinylidene difluoride Immobilon-P membrane (Millipore). After blocking, the membranes were incubated with primary antibodies as shown in Table 1. Secondary antibodies were horseradish peroxidase (HRP)-conjugated goat anti-mouse immunoglobulin (Ig), HRP-conjugated goat anti-rabbit Ig, and HRP-conjugated donkey anti-goat Ig (1:2,000; Santa Cruz Biotechnology). Bound immunocomplexes were detected using enhanced chemiluminescence detection reagents (GE Healthcare).

Immunofluorescence. Cells were seeded at 5×10^4 per 13-mm coverslip in a 24-well plate and cultured overnight. They were fixed in 4% paraformaldehyde and permeabilized with 0.1% Triton X-100. After blocking in 1% bovine serum albumin, the cells were incubated with primary antibodies as shown in Table 1. Secondary antibodies were Alexa Fluor 568–conjugated goat anti-mouse IgG, Alexa Fluor 488–conjugated donkey anti-mouse IgG, and Alexa Fluor 488–conjugated donkey anti-rabbit IgG (1:1,000; Molecular Probes, Invitrogen). All experiments were carried out in the absence of primary, secondary, or both antibodies as negative controls. DNA was stained with 50 μg/mL 4′,6-diamidino-2-phenylindole (DAPI; Molecular Probes). To visualize actin, 50 μg/mL phalloidin-TRITC (Sigma-Aldrich) was used. A series of optical sections were taken with a Zeiss LSM 510 confocal microscope and projected to single images using LSM 510 software (Zeiss). Identical acquisition methods were used for all samples to allow direct comparison of the resulting images.

2D-DIGE cell lysis and CyDye labeling. Cells were grown in 15-cm-diameter plates until 80% confluent and then serum starved for 24 h to prevent the appearance of highly abundant serum proteins on two-dimensional gels before lysing in two-dimensional lysis buffer [8 mol/L urea, 2 mol/L thiourea, 4% CHAPS, 0.5% IGEPAL CA-630, 10 mmol/L Tris (pH 8.3)]. All samples were homogenized by passing through a 21-gauge needle and cell debris was removed by centrifugation. Protein concentrations were determined using Coomassie Protein Assay Reagent (Perbio Science) and 150 μg of each sample were labeled with either NHS-Cy3 or NHS-Cy5 dyes as described previously (25). Cy3 and Cy5 were randomly assigned to biological quadruplicate samples from separately grown cultures and labeled samples were mixed with the same amount (150 μg) of a Cy2-labeled pool of all samples. NHS-Cy2 was purchased from GE Healthcare, whereas NHS-Cy3 and NHS-Cy5 were synthesized and stored in house (26). After labeling, the samples were randomly assigned to a specific gel and combined before separation. In total, six gels were run and 18 images were generated.

Combined samples were reduced with DTT (65 mmol/L final concentration) before the addition of carrier Ampholines/Pharmalyte mixture [final 2% (v/v)] and bromphenol blue. Finally, the volume was adjusted to 450 μL with two-dimensional lysis buffer and the samples were agitated before centrifugation.

2D-DIGE, fluorescence imaging, image analysis, spot picking, and tryptic digestion. The procedures were carried out in a dedicated clean room as described previously (25). Briefly, for the first dimension, 24-cm pH 3 to 10 nonlinear immobilized pH gradient strips (GE Healthcare) were used, and the second dimension was run in 12.5% homogenous SDS-PAGE gels bonded to low-fluorescence glass plates. Gels were run in Ettan12 gel tanks (GE Healthcare) overnight at 2.2 mA per gel and 16°C. They were scanned between glass plates using a Typhoon 9400 multiwavelength fluorescence imager using ImageQuant software (both from GE Healthcare) and the images were exported into DeCyder software v5.0 (GE Healthcare). Comparison of experimental (Cy3 or Cy5 labeled) spots with the corresponding standard Cy2-labeled spots gave a standardized abundance for each matched spot; the values were averaged across biological quadruplicates. Only spots displaying a >1.4 average fold increase or decrease in abundance between each condition, matching across all gel images and having P values of <0.05 (two-sided Student's t test), were selected for identification. Spot picking and tryptic digestion was done using modified porcine trypsin (Promega) as described previously (25).

Protein identification. Protein identification was achieved by liquid chromatography-tandem mass spectrometry (MS/MS) as described previously (25). Nano-high-performance liquid chromatography (HPLC) electrospray ionization (ESI) collision-induced dissociation MS/MS was done on an Ultimate HPLC with a PepMap C18 75-μm-inner diameter column (both Dionex) at a flow rate of 300 nL/min, coupled to a Q-TOF1 mass spectrometer (Micromass). Spectra were processed using MassLynx (Waters/Micromass) software and submitted to Mascot database search

Table 1. List of primary antibodies used in Western blotting and immunofluorescence

Primary antibody	Species raised in	Supplier	Dilution for Western blotting	Dilution for immunofluorescence
V5	Mouse	Invitrogen	1:5,000	N/A
KRT8	Mouse	Abcam	1:1,000	1:100
KRT8 phospho-Ser^{73}	Rabbit	Abcam	1:10,000	1:250
KRT8 phospho-Ser^{431}	Mouse	Abcam	1:200	1:100
KRT18	Mouse	Abcam	1:1,000	1:100
KRT18 phospho-Ser^{33}	Mouse	Abcam	1:200	1:100
KRT19	Mouse	Abcam	1:1,000	N/A
Cofilin	Rabbit	Abcam	1:15,000	N/A
Cofilin phospho-Ser^{3}	Rabbit	Abcam	1:1,000	N/A
GST	Goat	Abcam	1:5,000	N/A
Cathepsin D	Mouse	Abcam	1:5,000	N/A
Actin	Goat	Santa Cruz Biotechnology	1:2,000	N/A
KRT18 phospho-Ser^{52}	Rabbit	Santa Cruz Biotechnology	1:200	1:100
S100A6	Rabbit	DAKO	1:5,000	1:100
S100P	Mouse	BD Biosciences	N/A	1:25

Abbreviation: NA, not applicable.

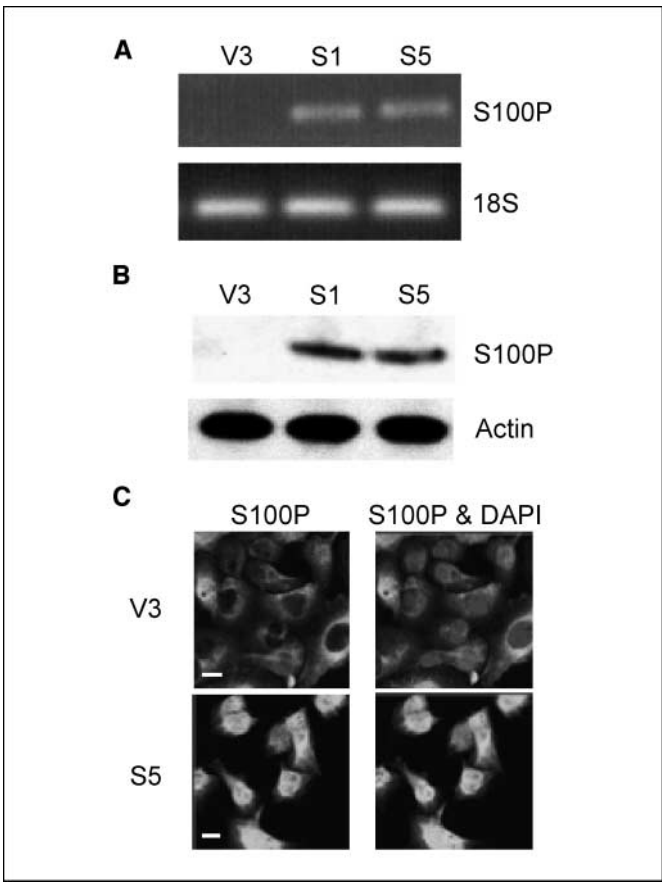

Figure 1. S100P overexpression in Panc1 pancreatic cancer cells. Panc1 cells were stably transfected with the pcDNA3.1/V5-His empty vector (clone V3) or pcDNA3.1/S100P-V5-His (clones S1 and S5). *A,* RT-PCR shows increased expression of S100P mRNA in S1 and S5 clones. 18S RT-PCR was used as a control. *B,* 20 μg of NP40 cell lysates were fractionated by SDS-PAGE and Western blotting was done using an anti-V5 antibody to show up-regulation of the V5-tagged S100P protein in S1 and S5 clones. Actin was used as a loading control. *C,* immunofluorescence shows increased expression of S100P in the S5 clone. Cells were labeled with an S100P antibody and an Alexa Fluor 488–labeled secondary antibody, and DAPI was used to stain the nuclei. *Bar*, 10 μm. Overexpression of S100P in S5 cells results in increased expression of S100P throughout the cells with a significant increase in nuclear staining. The pictures are representative of at least three experiments.

routines against the Human IPI database v3. Positive identifications were made when at least three peptide sequences matched an entry and MOWSE scores were above the significance threshold value ($P = 0.05$).

Wound-healing assay. Cells (1×10^6 per well) were plated in a six-well plate and cultured until confluent. A scratch was made to the monolayer with a 200 μL pipette tip and photographs (magnification, ×400) were taken immediately at 24 and 48 h after wounding. These were printed and the size of the wound was measured. Statistical analysis of the data was carried out using a paired Student's *t* test with a significance level of $P < 0.05$. Each experiment was done in triplicate.

Glutathione *S*-transferase pull-down assay. Glutathione *S*-transferase (GST)-tagged proteins were expressed from pGEX-S100P in the *Escherichia coli* strain pLysS (Promega) as described (14). Panc1 cells were lysed in CRB300 [20 mmol/L Tris (pH 8), 300 mmol/L NaCl, 0.5% NP40, 2 mmol/L DTT, 5 mmol/L $CaCl_2$ with protease inhibitors] and incubated with 10 μg S100P-GST or GST alone overnight at 4°C. Glutathione-Sepharose 4B (50 μL; GE Healthcare) was added and incubated at 4°C for 2 h. The samples were washed with CRB300 followed by CRB100 [20 mmol/L Tris (pH 8), 100 mmol/L NaCl, 0.5% NP40, 2 mmol/L DTT, 5 mmol/L $CaCl_2$ with protease inhibitors]. Bound target proteins were eluted in loading buffer (see above) and analyzed by immunoblotting.

Invasion assay. Invasion assays were done using Biocoat Matrigel Invasion Chambers with 8-μm pores (BD Biosciences). E4 medium (750 μL) supplemented with 10% FCS was added to the lower chamber and 2.5×10^4 cells in 500 μL serum-free medium were added to the upper chamber and incubated for 48 h at 37°C. Cells that moved through the pores were fixed in 100% methanol and stained with 1% Giemsa blue (Sigma-Aldrich). The membranes were photographed at ×100 magnification and the number of cells was counted. Statistical analysis was done using a paired Student's *t* test with a significance level of $P < 0.05$. Each experiment was repeated in triplicate.

Cathepsin D assay. Cells (1×10^5 per well) in 24-well plates were incubated with 100 μmol/L pepstatin A or DMSO as a negative control for 48 h. Cells were lysed in 10 mmol/L Tris (pH 7.4), 1.5 mmol/L EDTA, and 0.1% thioglycerol (27). Cell lysate (10 μL) was incubated with 80 μL sodium acetate (pH 4.0) and 10 μL 200 μmol/L fluorogenic cathepsin D substrate solution (Merck) at 40°C for 10 min. The reaction was then terminated with 5% trichloroacetic acid. Cathepsin D activity was measured at an excitation of 328 nm and emission of 393 nm using a Hitachi F-4500 Fluorimeter. Statistical analysis of the data was done using a paired Student's *t* test with a significance level of $P < 0.05$.

Pathway analysis. Ingenuity Pathway analysis (IPA) is a web-based application[3] that builds biological networks based on entered data and published associations. Proteins displaying altered expression levels in S100P-overexpressing cells were designated as focus genes and searched (with their corresponding fold change values) against published data using IPA. Scores were generated for each network and show the likelihood that proteins associated with the focus genes have been selected by random chance (e.g., a score of 2 gives a 99% confidence, with higher scores signifying greater confidence). Based on these scores, IPA prioritizes the networks, identifies the associated genes, and assigns the most significant biological functions to each network. The global functional analysis feature calculates this significance using the right-tiled Fisher's exact test, with a *P* value of <0.05 being significant.

Results

Establishment of S100P-overexpressing stable cell lines. Stable cell lines were established in which S100P was overexpressed from the pcDNA3.1/S100P-V5-His plasmid or containing the empty vector pcDNA3.1/V5-His as a negative control. Six pcDNA3.1/S100P-V5-His and three pcDNA3.1/V5-His single-cell clones were isolated; the two clones with the highest levels of S100P, S1 and S5, along with one arbitrarily selected empty vector control clone, V3, were analyzed further. S100P overexpression in S1 and S5, in comparison with the V3 control clone, was confirmed at the mRNA level by RT-PCR using S100P-specific primers (Fig. 1*A*). Western blotting using a V5 antibody to detect the tagged S100P protein confirmed overexpression at the protein level (Fig. 1*B*). Immunofluorescence using an S100P antibody detected low endogenous expression of S100P in V3 control cells, which was mainly cytoplasmic (Fig. 1*C*). However, S100P staining in S5 (Fig. 1*C*) and S1 (data not shown) was more intense and predominantly nuclear, with 92% of S5 cells displaying nuclear staining compared with 9% of V3 cells (a minimum of 150 cells was counted for each clone).

Expression profiling using 2D-DIGE and MS. A master gel image, created using Photoshop CS2 software (Fig. 2*A*), shows the positions of protein spots that displayed changes in expression between the vector control and S100P-overexpressing cells. Some areas of the image have been expanded to show more detail of specific protein changes. Image analysis using DeCyder software v5.0 identified 52 protein spots that displayed differential expression. Subsequent MS/MS analysis resulted in 45 identifications at high confidence (7 spots failed our validation criteria); of these,

[3] http://www.Ingenuity.com

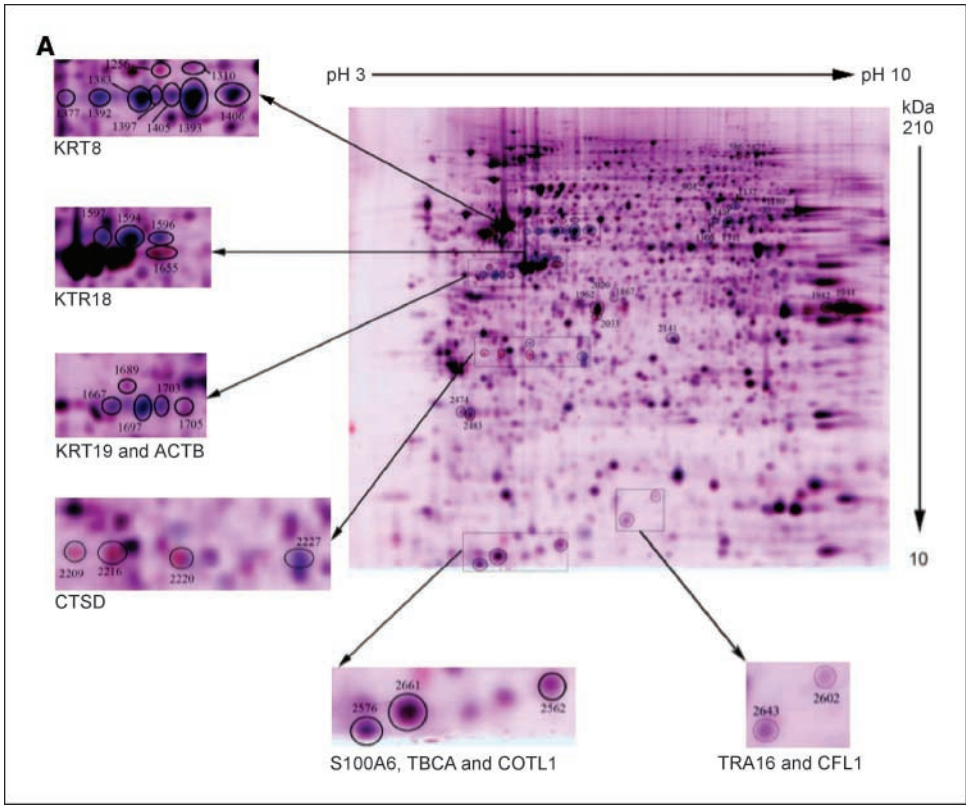

Figure 2. Results of 2D-DIGE analysis. *A,* representative gel image displaying protein spots with S100P-dependent changes in expression. Representative data of two pseudocolored images of vector only sample (*blue*, Cy5) and S100P-overexpressing sample (*red*, Cy3) created in Photoshop. *Circled numbers,* positions of differentially expressed spots selected by DeCyder software that were subsequently identified with high confidence by Nano-HPLC-ESI-MS/MS. Magnified regions show some of the differentially expressed proteins that were confirmed in this study. *CTSD,* cathepsin D.

40 spots yielded a single identification with 23 unique gene products, 10 of which were up-regulated, 12 were down-regulated, and 1 was both up-regulated and down-regulated. The differentially expressed proteins for the S5 clone are listed in Fig. 2*B*. Both S1 and S5 clones displayed the same pattern of regulation for all the proteins listed (data for both clones are shown in Supplementary Table S1A–C). Detailed lists showing search scores, sequence coverage, IPI, and UniGene IDs, as well as the remaining spots that contained multiple identifications, are shown in Supplementary Table S1A–C.

The functional classification of all differentially expressed proteins in our data set is represented in Fig. 2*C*. The classification is based on the gene ontology annotation in the Kyoto Encyclopedia of Genes and Genomes database[4] and IPI human database.[5] The majority (86%) of differentially regulated proteins fell within three major functional groups, structure/motility, metabolism, and protein processing, with proteins involved in structure/motility representing the largest functional group with 21 isoform entries (9 gene products). Primary among the structure/motility group were cytokeratins 8 (KRT8), 18 (KRT18), and 19 (KRT19); actin (ACTB); cofilin (CFL1); and coactosin-like 1 (COTL1) protein. KRT8 was identified as a series of spots with similar molecular weight but differing isoelectric points (pI; Fig. 2*A*). A similar pattern of separation was also noted for KRT18 and KRT19 and is suggestive of post-translational modifications. A database search specific for phosphorylation of serine, threonine, or tyrosine residues was conducted on the complete data set. This revealed phosphorylation of a single peptide derived from KRT8 on S26 and the corresponding nonphosphorylated peptide within spot number 1392 (Supplementary Fig. S1). Whereas KRT19 spot 1697 contained a single phosphorylated peptide (S35), KRT19 spot 1705 contained the corresponding unphosphorylated peptide (Supplementary Fig. S1). An isoform of ACTB was found to be down-regulated in 2D-DIGE; however, Western blot analysis did not show any change in total protein levels of actin (Fig. 1*B*). Cofilin (spot number 2602) was identified in the region of pH 5 to 6, which is well below the expected theoretical pI of 8.26. This positional shift is highly indicative of a change in phosphorylation.

In addition to the described cytoskeletal changes, we further show that S100P overexpression leads to significant changes in cathepsin D expression. Cathepsin D was identified on the gel in a row of four spots spanning several pH units (Fig. 2*A*, spots 2209, 2216, 2220, and 2227), which could be indicative of post-translational modification(s). The three cathepsin D spots that seem to increase in abundance in S100P-overexpressing cell lines are likely to represent complex post-translational modifications in comparison with the down-regulated spot, which is a form with fewer (or no) post-translational modifications. Several metabolic enzymes, such as glyceraldehyde-3-phosphate dehydrogenase (GAPDH), LDHB, PYGB, TALDO1, ALDHIA3, and glucose-6-phosphate dehydrogenase, were also identified, as well as another S100 protein, S100A6.

Validation and characterization of protein changes. Western blotting and immunofluorescence were used to confirm the 2D-DIGE results. Immunoblotting showed reduced levels of KRT8, KRT18, and KRT19 in S100P-overexpressing cells (Fig. 3*A*). Furthermore, there seemed to be a change in the distribution of the cytokeratins, with less protein present in the soluble cell fraction compared with the insoluble fraction in S100P-overexpressing cells (Fig. 3*B*). Western blotting using phosphospecific antibodies (KRT8 S73 and S431, KRT18 S33 and S52) revealed a similar pattern

[4] http://www.genome.jp/kegg/kegg2.html
[5] http://www.ebi.ac.uk/IPI/IPIhuman.html

B

Spot	Protein Name	Fold chan
586	Glycogen phosphorylase brain type	+1.51
587	Elongation factor 2	+1.62
904	Tumour necrosis factor type 1 receptor-associated protein	+1.59
1256	Peptidyl-prolyl *cis*-trans isomerase	+1.66
1867	Transaldolase	+1.53
1934	Glyceraldehyde-3-phosphate dehydrogenase	+1.60
1942	Glyceraldehyde-3-phosphate dehydrogenase	+1.49
1982	L-lactate dehydrogenase – B chain	+1.41
2020	L-lactate dehydrogenase – B chain	+1.65
2209	**Cathepsin D**	+1.56
2216	**Cathepsin D**	+2.76
2220	**Cathepsin D**	+2.44
2483	Tumor protein translationally controlled 1	+1.61
2576	**S100 calcium-binding protein A6**	+3.13
2602	**Cofilin 1**	+1.63
1132	EH domain-containing protein	-1.63
1180	Catalase	-1.71
1241	Aldehyde dehydrogenase IA3	-1.66
1306	Glucose-6-phosphate 1 dehydrogenase	-1.65
1310	**Keratin 8**	-2.00
1311	Glucose-6-phosphate 1 dehydrogenase	-1.71
1377	**Keratin 8**	-1.99
1383	**Keratin 8**	-2.70
1392	**Keratin 8**	-2.75
1393	**Keratin 8**	-2.14
1397	**Keratin 8**	-2.99
1405	**Keratin 8**	-2.70
1406	**Keratin 8**	-2.79
1594	**Keratin 18**	-2.14
1596	**Keratin 18**	-3.33
1667	**Keratin 19**	-1.50
1689	**Actin**	-2.03
1697	**Keratin 19**	-1.68
1703	**Keratin 19**	-2.02
1705	**Keratin 19**	-3.22
2141	Δ3,5-Δ2,4-dienoyl-CoA isomerase	-1.56
2227	**Cathepsin D**	-2.75
2562	Coactosin 1-like	-1.41
2643	TR4 orphan receptor-associated protein	-1.57
2661	Tubulin-specific chaperone A	-1.55

C

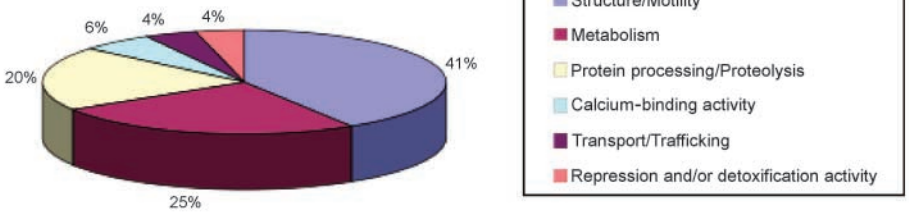

Figure 2 *Continued. B,* list of up-regulated (+) and down-regulated (−) proteins from 2D-DIGE analysis. *C,* pie chart showing the functional classification of all identified proteins.

of expression as seen when using antibodies raised against the whole protein. This suggests that there were little or no changes in the overall level of phosphorylation at these sites due to S100P overexpression (Fig. 3*A* and *B*). However, when immunofluorescence was used to examine the expression and structure of the cytokeratins, an overall decrease in the organization of KRT8, KRT18, and KRT19 was observed in S100P-overexpressing cells compared with vector controls (Fig. 3*C* and *D*; data for KRT19 not shown). Furthermore, changes were also seen in the structure of phosphorylated cytokeratins; for example, when using a KRT8 phosphospecific S431 antibody, a punctate staining was observed in S1 and S5 cells (particularly within the nucleus)

that was not seen in control V3 cells, whereas with the KRT18 phosphospecific antibodies for S33 an almost total loss of structural organization was observed in the S100P-overexpressing cells, with the protein distributed throughout the cytoplasm and taking on more of a grainy appearance.

A spot containing the actin-depolymerizing and actin-severing protein cofilin was up-regulated in our 2D-DIGE analysis. Western blotting did not show any changes in the total amount of cofilin protein in S100P-overexpressing cells (Fig. 4*A*). However, a change in the phosphorylation status of cofilin was apparent using an antibody raised against cofilin phosphorylated S3, the major site involved in blocking the actin-binding activity of cofilin. A significant increase in phosphorylated S3 was detected in the insoluble fraction of NP40 lysates (Fig. 4*A*).

Immunofluorescence staining for filamentous actin showed a typical actin structure with cortical actin expression and stress fibers in control V3 cells (representative images from three experiments are shown in Fig. 4*B*), whereas in the majority of S5 cells a more punctate staining was observed, with a decrease in the level of cortical actin staining and the number of cells containing stress fibers (Fig. 4*B*). As these changes are indicative of active reorganization of the actin cytoskeleton (28), the functional significance of this was investigated further using a wound-healing assay. Closure of the wound in S100P-overexpressing cells was more complete after 48 h compared with the V3 control cells (a representative image is shown in Fig. 4*C* and a summary of three experiments is shown in Fig. 4*D*), showing that S100P-overexpressing cells are more motile.

Increased S100A6 expression in S100P-overexpressing cell lysates was also confirmed by Western blotting (Fig. 5*A*) and immunofluorescence, where it was shown to be mostly colocalized with S100P in the nuclei (Fig. 5*B*). To investigate this colocalization further, we carried out GST pull-down assays using GST-tagged S100P and showed that S100P-GST could bind S100A6 from Panc1 cell lysates (Fig. 5*C*), supporting the possibility of an interaction between the two proteins *in vivo*.

Cathepsin D can exist in three forms: unprocessed preprocathepsin D, partially processed procathepsin D, and enzymatically

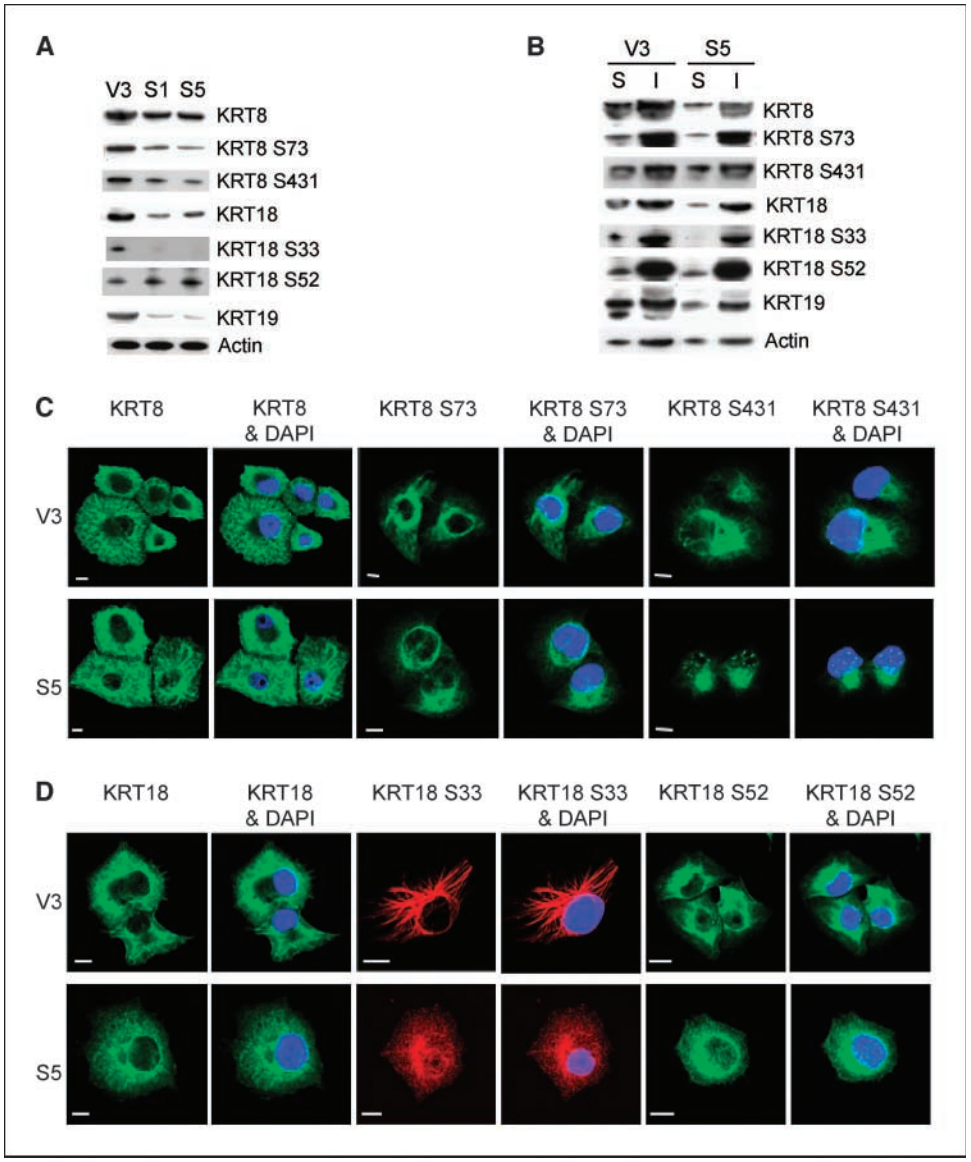

Figure 3. Validation of cytokeratin deregulation. *A,* 10 μg of Triton X-100 cell lysates were fractionated by SDS-PAGE and Western blotting was used to detect the expression levels of KRT8, phospho-S73 KRT8, phospho-S431 KRT8, KRT18, phospho-S33 KRT18, phospho-S52 KRT18, and KRT19, and actin was used as a loading control. Decreased expression of KRT8, KRT18, and KRT19 was observed in S100P-overexpressing cells. *B,* Western blots were also carried out using soluble and insoluble fractions of NP40 cell lysates. Soluble (10 μg) and insoluble (10 μL) NP40 cell lysates were fractionated by SDS-PAGE and subjected to Western blotting using the cytokeratin antibodies used in (*A*), and actin was used as a loading control. In S100P-overexpressing cell lysates, the majority of the cytokeratins are present in the insoluble cell fractions. *C,* immunofluorescence using KRT8, phospho-S73 KRT8, and phospho-S431 KRT8 primary antibodies and an Alexa Fluor 488–labeled secondary antibody, and DAPI was used to stain the nuclei. *Bar*, 10 μm. The pictures are representative of at least three experiments. *D,* immunofluorescence using KRT18, phospho-S33 KRT18, and phospho-S52 KRT18 primary antibodies and Alexa Fluor 488–labeled (*green*) and Alexa Fluor 568–labeled (*red*) secondary antibodies. DAPI was used to stain the nuclei. *Bar*, 10 μm. The pictures are representative of at least three experiments.

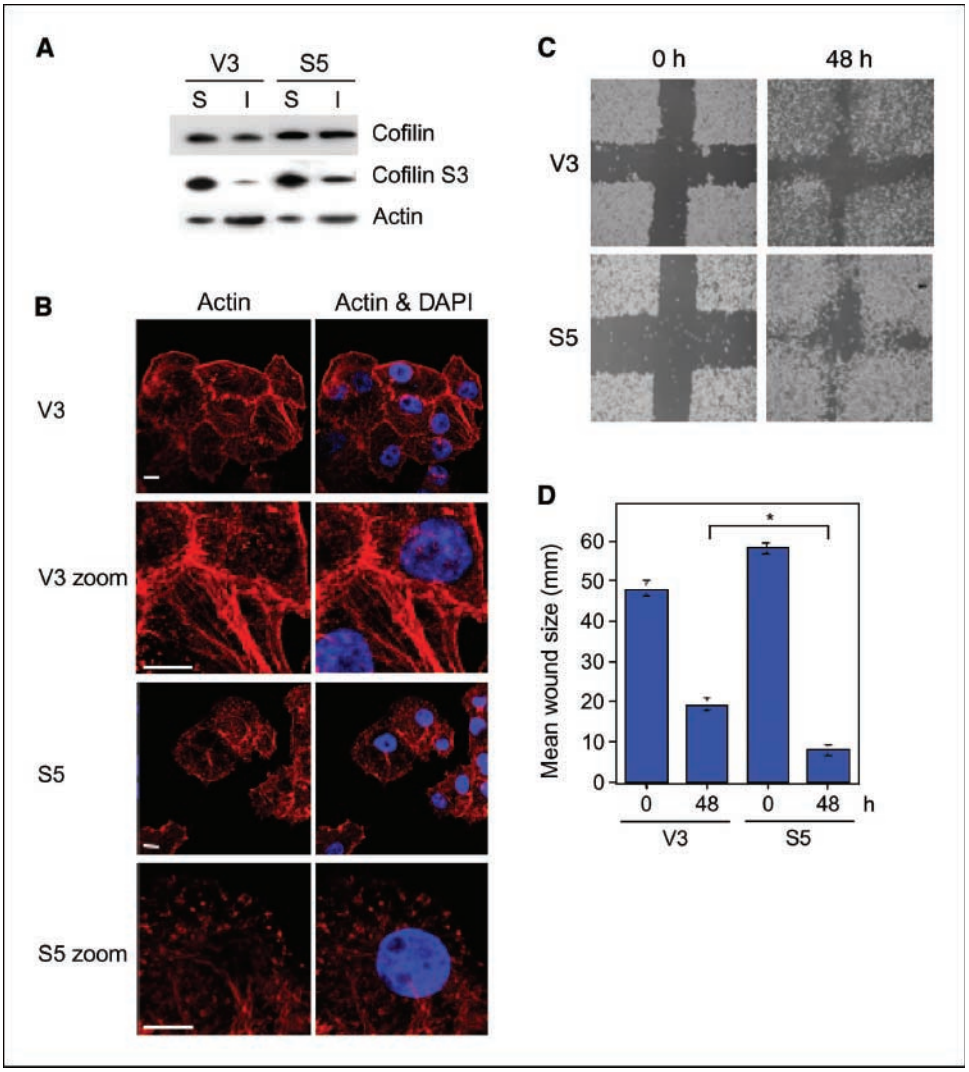

Figure 4. Cofilin deregulation and actin immunofluorescence. *A,* Western blot showing expression of cofilin and phospho-cofilin S3 in soluble and insoluble cell fractions. Soluble (10 μg) and insoluble (10 μL) NP40 cell lysates were fractionated by SDS-PAGE and subjected to Western blotting using cofilin, phospho-cofilin S3, and actin antibodies. Overall cofilin protein levels are unchanged between V3 and S5 samples; however, there is an increase in phosphorylation of cofilin at S3 in the S100P-overexpressing cell lysates. *B,* V3 and S5 were stained with phalloidin to visualize actin (*red*) and DAPI was used to highlight the nuclei. Disruption of the actin cytoskeleton was observed in S5, with a reduction in the number of stress fibers and in cortical actin expression. *Bar*, 10 μm. The zoom figures are magnified regions from the figures above showing actin stress fibers in V3 and the punctate actin distribution in S5 cells. The pictures are representative of at least three experiments. *C,* wound-healing assays showing V3 and S5 cells at 0 and 48 h after wounding; representative images from triplicate experiments are shown. *D,* bar chart showing the size of the wound at 0 and 48 h, measured in millimeters from ×400 magnification photographs; representative data from one of the triplicate experiments are shown.

active cathepsin D. Western blot analysis showed a significant increase in expression of the preproisoforms and proisoforms of cathepsin D in S100P-overexpressing clones compared with control cells with a slight increase seen in expression of the active form of cathepsin D (Fig. 6*A*). The preproisoforms and proisoforms of cathepsin D have been implicated in the invasive potential of cancer cells (29, 30). We therefore carried out invasion assays to investigate the contribution of cathepsin D to the invasive potential of S100P-overexpressing cells. We observed a significant increase in the invasion of S100P-overexpressing clones, with a greater than 2-fold increase in the number of invading cells compared with vector only controls (Fig. 6*B*). To examine the role of cathepsin D in the invasive potential of S100P-overexpressing cells, we examined its activity using a fluorogenic assay, which showed significantly higher cathepsin D activity in S100P-overexpressing cell lysates compared with vector only control lysates (Fig. 6*C*). Following treatment with 100 μmol/L of the cathepsin D inhibitor pepstatin A for 48 h, activity of cathepsin D in S100P-overexpressing cells was reduced to similar levels as observed in control cells (Fig. 6*C*). Therefore, we repeated the cell invasion assays following treatment with pepstatin A. This showed a significant decrease in the number of invading cells after inhibition of cathepsin D activity, with the numbers reduced to a level similar to that observed for the control cell line (Fig. 6*D*). This suggests that the increased invasive potential of S100P-overexpressing cells is at least partly due to the resulting increase in cathepsin D expression.

Pathway analysis. IPA generated two biological networks with highly significant scores: network 1 had 13 focus genes and a score of 27 and network 2 contained 4 focus genes with a score of 7 (Supplementary Fig. S2*A–C*). Supplementary Figure S2*A* displays the gene content, scores, and number of focus genes in each network, with focus genes highlighted in red (up-regulated) or green (down-regulated). The remaining gene products represent additional associated genes identified by IPA. The top functions associated with these two biological networks were cellular assembly and organization (8 proteins; significance value, 4.65×10^{-6} to 3.48×10^{-2}), cell death (13 proteins; significance value, 4.65×10^{-6} to 3.19×10^{-2}), and cancer (9 proteins; significance value, 2.21×10^{-3} to 3.48×10^{-2}).

Discussion

In this study, we have used 2D-DIGE to quantitate proteins with altered expression following up-regulation of S100P expression in the pancreatic cancer cell line Panc1. The identification and subsequent functional classification of these proteins indicated

that a high number were associated with cytoskeletal changes. Although identification of structural/motility proteins is a common motif in proteomic experiments, the level of their involvement warranted further in-depth investigation.

The cytoskeleton is composed of an intricate and highly dynamic network of actin, tubulin, and intermediate filaments. Increased expression of S100P led to a reduction in cortical actin, disorganization of stress fibers, and the appearance of punctate cytoplasmic accumulations. Furthermore, we show the concomitant deregulation of COTL1 and cofilin, proteins that both bind to and regulate filamentous actin. Whereas little is known about COTL1, the role of cofilin as a key regulator of actin polymerization is well established (31) and increased activity of cofilin has been directly correlated with invasion and metastasis (32). A change in the phosphorylation status of cofilin, suggested by a shift in two-dimensional gel position, was confirmed using an S3 phosphospecific antibody. This, in association with the observed changes to the actin cytoskeleton, suggests a state of dynamic flux within the actin filaments, which is critical for migratory cell behavior. Pathway analysis additionally highlighted several other proteins that directly or indirectly regulate actin dynamics, such as LIMK1 (a cofilin regulatory kinase) and ezrin (VIL2), an essential actin bundling protein, which is a direct binding partner of S100P (33).

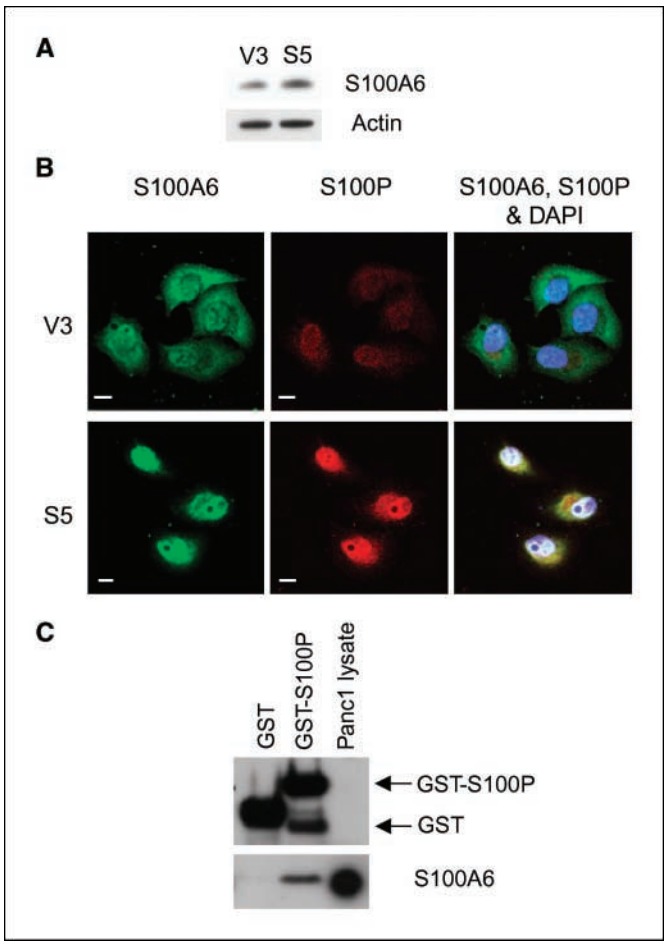

Figure 5. Expression of S100A6 in S100P-overexpressing cells. *A,* Western blotting shows increased expression of S100A6 in S100P-overexpressing cell lysates compared with vector controls. NP40 cell lysates (10 μg) were fractionated by SDS-PAGE and subjected to Western blotting using an S100A6 antibody, and actin was used as a loading control. *B,* immunofluorescence showing colocalization of S100P and S100A6 in cells overexpressing S100P. Primary antibodies against S100A6 and S100P were used with Alexa Fluor 488–labeled (*green*) and Alexa Fluor 568–labeled (*red*) secondary antibodies, respectively. DAPI was used to stain the nuclei. *Bar*, 10 μm. The pictures are representative of at least three experiments. *C,* S100P interacts with S100A6 in GST pull-down assays. GST or GST-S100P pull-down samples (35 μL) were fractionated by SDS-PAGE along with 5 μg Panc1 NP40 cell lysate as a control. Western blots were carried out using GST and S100A6 antibodies.

S100P overexpression led to disruption of the structure of KRT8, KRT18, and KRT19, which are the major intermediate filaments of the exocrine pancreas (34). It has been firmly established that cytokeratins not only provide mechanical support to preserve the cytoarchitecture but are also involved in modulating multiple signaling proteins (35). For example, the actin-ezrin scaffold cannot assemble in the absence of intermediate filaments (36), and cytokeratins are important regulators of cell migration (37). The organization of intermediate filaments is regulated by several post-translational modifications, including phosphorylation (35, 38, 39). Alterations to the phosphorylation status of cytokeratins can modify their cellular distribution, assembly, and solubility, resulting in functional changes (35).

Our study provides evidence of post-translational modifications of KRT8, KRT18, and KRT19 following overexpression of S100P. As S100 proteins are known to regulate protein phosphorylation (4), S100P may also regulate the phosphorylation of these cytokeratins in pancreatic cancer. The observed redistribution of cytokeratins from the soluble to the insoluble cell fraction suggests a shift toward incorporation of these proteins into complex insoluble structures. Large intermediate filament complexes have different viscoelastic properties that make the cell more resistant to mechanical stress (40) and therefore influence survival and migration of the invasive cell (37, 40). The role of intermediate filaments in migration, invasion, and metastasis has been established in several cancer types (41).

Several S100 proteins have previously been shown to interact with the cytoskeleton (42), including S100A1 and S100A4, both of which are strongly associated with actin stress fibers in vascular smooth muscle cells (43). S100A8 and S100A9 colocalize with the intermediate filament vimentin in monocytes (44), whereas antisense inhibition of S100B causes changes in cell morphology and differences in actin distribution and organization in glial cells (45). We have now shown that S100P also has an effect on the cytoskeleton in pancreatic cancer cells.

Overexpression of S100P led to increased levels of S100A6. These proteins were initially coisolated from placenta (5), and their pattern of expression is similar in PanINs and PDAC (12, 15). S100A6 has also been implicated in the motility and invasion of pancreatic cancer cells (46) and is inversely correlated with patient prognosis (16). We have shown that S100P and S100A6 colocalize in Panc1 cells and that S100P can associate with S100A6 in GST pull-down assays. These results suggest that S100P may dimerize with S100A6 *in vivo*, although this requires further confirmation. We have also observed relocalization of S100P and S100A6 to the nucleus following overexpression of S100P, but the physiologic relevance of this has yet to be determined.

The observed changes in cytokeratins and actin are most likely to contribute to the increased cellular motility of S100P-overexpressing cells. However, motility alone does not explain the highly invasive nature of this disease. Herein, we show that S100P overexpression leads to significant changes in the preproforms and proforms of cathepsin D with a smaller increase in the catalytically active form. Cathepsin D expression is up-regulated in several cancer types, including PDAC (30, 47, 48), and plays a crucial role in proteolytic degradation of extracellular matrix (ECM), which

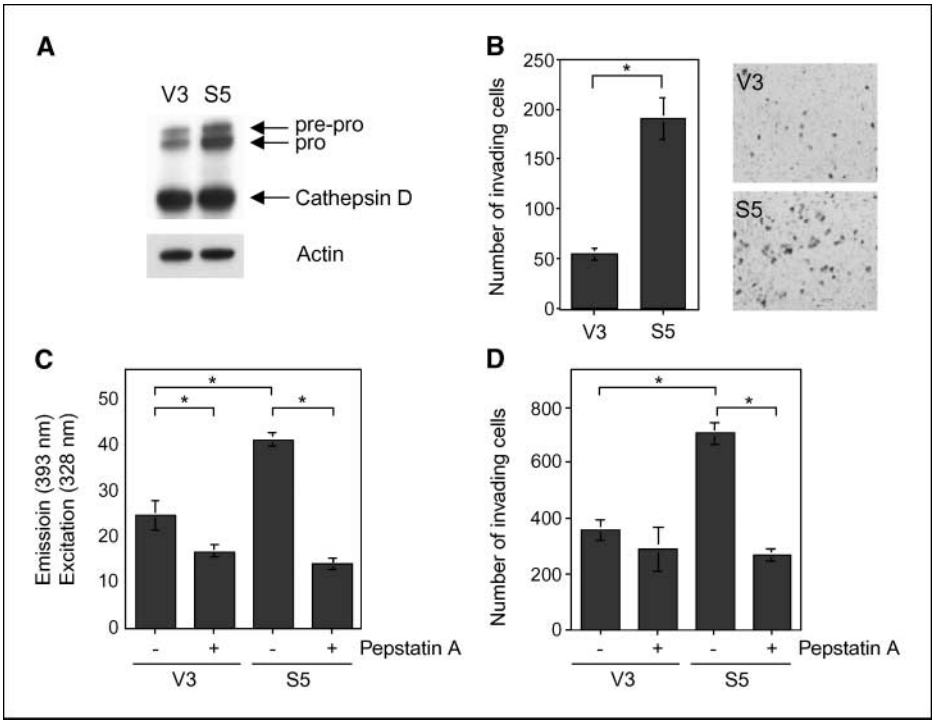

Figure 6. Expression of cathepsin D in S100P-overexpressing cells. *A,* 10 μg of Triton X-100 cell lysates were fractionated by SDS-PAGE and Western blotting was used to detect expression of cathepsin D. Actin was used as a loading control. Several cathepsin D isoforms were detected: preprocathepsin D at 52 kDa, precathepsin D at 44 kDa, and cathepsin D at 32 kDa. *B,* invasion assays show the increased invasive potential of S100P-overexpressing cells compared with vector controls, and mean values of triplicate experiments are shown. *C,* cathepsin D assay using 10 μL V3 and S5 cell lysates following treatment with 100 μmol/L pepstatin A or DMSO as a negative control for 48 h, and mean values of triplicate experiments are shown. *D,* invasion of S100P-overexpressing cells and empty vector controls was examined following inhibition of cathepsin D activity by 100 μmol/L pepstatin A for 48 h, and mean values of triplicate experiments are shown.

can be completely abrogated following treatment with the inhibitor pepstatin (49). The correlation between procathepsin D secretion and the ability of cells to invade has been shown previously (29, 30), and cathepsin D overexpression has been associated with poor prognosis in breast (50, 51), prostate (52), and cervical cancer (53). Interestingly, we have observed high expression levels of both S100P and cathepsin D in PaTu 8988s cells in comparison with PaTu 8988t. These cells were isolated from the same primary human pancreatic adenocarcinoma (54), and whereas PaTu 8988s is poorly differentiated and highly invasive when injected i.v. into nude mice, PaTu 8988t is well differentiated and does not metastasize (54). The contribution of S100P and cathepsin D to the invasive potential of PaTu 8988s cells is currently being investigated in more detail.

Our results suggest a degree of cooperativity between the changes in structure that allow greater motility and the associated ability to degrade the ECM represented by increased cathepsin D expression. Such a mode of action has already been suggested, where highly invasive carcinoma cells form membrane protrusions called invadopodia that have the capacity to degrade the underlying matrix (55). Proteases are secreted and activated at invadopodia sites, and these sites correspond exactly to areas of ECM degradation (56). However, whether this is also the case in pancreatic cancer needs to be investigated further.

When all differentially expressed proteins were introduced into IPA, two signaling networks that were easily merged were compiled; the first one illustrated the observed cytoskeletal changes with connection of S100P to cytokeratins through ezrin (VIL2; Supplementary Fig. S2*A*), whereas the other indicated a potentially important link between S100A6, GAPDH, and cathepsin D through Myc-dependent expression (Supplementary Fig. S2*B*). C-myc is overexpressed in ~30% of PDAC cases (57) and is up-regulated, along with S100P, in mucinous cystic neoplasms, which are additional precursor lesions to PDAC (58). IPA also highlighted the complex transcriptional regulation potentially underlying the observed changes (Supplementary Fig. S2*B* and *C*). This is even more clearly presented in the cellular layout mode, where each protein is located in its *in vivo* context (Supplementary Fig. S2*C*), and offers a future direction for exploring the roles of nuclear S100P, which are currently completely unknown.

The remaining proteins that were affected by S100P overexpression, such as SMARCD2, TPT1, TRAP1, and FKBP4, and several enzymes were not investigated further. However, they may offer a molecular basis to explain additional functions of S100P and therefore warrant confirmatory validation.

In summary, our study provides an insight into the intracellular events following S100P up-regulation *in vitro*: we show that S100P plays a critical role in the maintenance of cytoskeletal reorganization/remodeling and the motile/invasive properties of pancreatic cancer cells. As up-regulation of S100P is seen in a clinical setting (19), we believe that at least some of the molecular changes described here recapitulate the *in vivo* situation; indeed, blocking of S100P expression significantly reduced the invasion of tumor cells in a pancreatic cancer mouse model (17, 18). S100P and S100A6 are expressed early in the development of PDAC, and both proteins are involved in the invasive process. This suggests that the micrometastatic signature is encoded early in the development of PDAC and could explain the almost invariable recurrence and devastating prognosis of this disease.

Acknowledgments

Received 2/8/2007; revised 5/25/2007; accepted 7/6/2007.

Grant support: Higher Education Funding Council for England (H.J. Whiteman and T. Crnogorac-Jurcevic), Cancer Research UK (M.E. Weeks, S.E. Dowen, and N.R. Lemoine), Research Advisory Board PhD Scholarship (S. Barry), and Ludwig Institute for Cancer Research (J.F. Timms).

The costs of publication of this article were defrayed in part by the payment of page charges. This article must therefore be hereby marked *advertisement* in accordance with 18 U.S.C. Section 1734 solely to indicate this fact.

We thank John Sinclair (University College London) for technical assistance with 2D-DIGE, Dr. Rathi Gangeswaran (Cancer Research UK Clinical Centre at Barts and The London) and Dr. Stephanie Kermorgant (Queen Mary University of London) for assistance with confocal microscopy, and Dr. Emmanuelle Liaudet-Coopman (Montpellier University) for the assistance with the cathepsin D assay.

References

1. Winter JM, Cameron JL, Campbell KA, et al. 1423 pancreaticoduodenectomies for pancreatic cancer: a single-institution experience. J Gastrointest Surg 2006; 10:1199–210; discussion 210–1.
2. Jemal A, Siegel R, Ward E, Murray T, Xu J, Thun MJ. Cancer statistics, 2007. CA Cancer J Clin 2007;57: 43–66.
3. Warshaw AL, Fernandez-del Castillo C. Pancreatic carcinoma. N Engl J Med 1992;326:455–65.
4. Donato R. S100: a multigenic family of calcium-modulated proteins of the EF-hand type with intracellular and extracellular functional roles. Int J Biochem Cell Biol 2001;33:637–68.
5. Becker T, Gerke V, Kube E, Weber K. S100P, a novel Ca^{2+}-binding protein from human placenta. cDNA cloning, recombinant protein expression and Ca^{2+} binding properties. Eur J Biochem 1992;207:541–7.
6. Dowen SE, Crnogorac-Jurcevic T. S100 proteins in cancer. Calcium Binding Proteins 2006;1:143–9.
7. Guerreiro Da Silva ID, Hu YF, Russo IH, et al. S100P calcium-binding protein overexpression is associated with immortalization of human breast epithelial cells *in vitro* and early stages of breast cancer development *in vivo*. Int J Oncol 2000;16:231–40.
8. Bertram J, Palfner K, Hiddemann W, Kneba M. Elevated expression of S100P, CAPL and MAGE 3 in doxorubicin-resistant cell lines: comparison of mRNA differential display reverse transcription-polymerase chain reaction and subtractive suppressive hybridization for the analysis of differential gene expression. Anticancer Drugs 1998;9:311–7.
9. Mousses S, Bubendorf L, Wagner U, et al. Clinical validation of candidate genes associated with prostate cancer progression in the CWR22 model system using tissue microarrays. Cancer Res 2002;62:1256–60.
10. Wang G, Platt-Higgins A, Carroll J, et al. Induction of metastasis by S100P in a rat mammary model and its association with poor survival of breast cancer patients. Cancer Res 2006;66:1199–207.
11. Beer DG, Kardia SL, Huang CC, et al. Gene-expression profiles predict survival of patients with lung adenocarcinoma. Nat Med 2002;8:816–24.
12. Crnogorac-Jurcevic T, Missiaglia E, Blaveri E, et al. Molecular alterations in pancreatic carcinoma: expression profiling shows that dysregulated expression of S100 genes is highly prevalent. J Pathol 2003;201: 63–74.
13. Buchholz M, Braun M, Heidenblut A, et al. Transcriptome analysis of microdissected pancreatic intraepithelial neoplastic lesions. Oncogene 2005;24: 6626–36.
14. Dowen SE, Crnogorac-Jurcevic T, Gangeswaran R, et al. Expression of S100P and its novel binding partner S100PBPR in early pancreatic cancer. Am J Pathol 2005; 166:81–92.
15. Shekouh AR, Thompson CC, Prime W, et al. Application of laser capture microdissection combined with two-dimensional electrophoresis for the discovery of differentially regulated proteins in pancreatic ductal adenocarcinoma. Proteomics 2003;3:1988–2001.
16. Vimalachandran D, Greenhalf W, Thompson C, et al. High nuclear S100A6 (Calcyclin) is significantly associated with poor survival in pancreatic cancer patients. Cancer Res 2005;65:3218–25.
17. Arumugam T, Ramachandran V, Logsdon CD. Effect of cromolyn on S100P interactions with RAGE and pancreatic cancer growth and invasion in mouse models. J Natl Cancer Inst 2006;98:1806–18.
18. Arumugam T, Simeone DM, Van Golen K, Logsdon CD. S100P promotes pancreatic cancer growth, survival, and invasion. Clin Cancer Res 2005;11:5356–64.
19. Ohuchida K, Mizumoto K, Egami T, et al. S100P is an early developmental marker of pancreatic carcinogenesis. Clin Cancer Res 2006;12:5411–6.
20. Liu N, Furukawa T, Kobari M, Tsao MS. Comparative phenotypic studies of duct epithelial cell lines derived from normal human pancreas and pancreatic carcinoma. Am J Pathol 1998;153:263–9.
21. Gharbi S, Gaffney P, Yang A, et al. Evaluation of two-dimensional differential gel electrophoresis for proteomic expression analysis of a model breast cancer cell system. Mol Cell Proteomics 2002;1:91–8.
22. Tonge R, Shaw J, Middleton B, et al. Validation and development of fluorescence two-dimensional differential gel electrophoresis proteomics technology. Proteomics 2001;1:377–96.
23. Unlu M, Morgan ME, Minden JS. Difference gel electrophoresis: a single gel method for detecting changes in protein extracts. Electrophoresis 1997;18: 2071–7.
24. Lieber M, Mazzetta J, Nelson-Rees W, Kaplan M, Todaro G. Establishment of a continuous tumor-cell line (panc-1) from a human carcinoma of the exocrine pancreas. Int J Cancer 1975;15:741–7.
25. Weeks ME, Sinclair J, Butt A, et al. A parallel proteomic and metabolomic analysis of the hydrogen peroxide- and Sty1p-dependent stress response in *Schizosaccharomyces pombe*. Proteomics 2006;6:2772–96.
26. Chan HL, Gaffney PR, Waterfield MD, et al. Proteomic analysis of UVC irradiation-induced damage of plasma proteins: serum amyloid P component as a major target of photolysis. FEBS Lett 2006;580: 3229–36.
27. Beaujouin M, Baghdiguian S, Glondu-Lassis M, Berchem G, Liaudet-Coopman E. Overexpression of both catalytically active and -inactive cathepsin D by cancer cells enhances apoptosis-dependent chemosensitivity. Oncogene 2006;25:1967–73.
28. Mitchison TJ, Cramer LP. Actin-based cell motility and cell locomotion. Cell 1996;84:371–9.
29. Johnson MD, Torri JA, Lippman ME, Dickson RB. The role of cathepsin D in the invasiveness of human breast cancer cells. Cancer Res 1993;53:873–7.
30. Laurent-Matha V, Maruani-Herrmann S, Prebois C, et al. Catalytically inactive human cathepsin D triggers fibroblast invasive growth. J Cell Biol 2005; 168:489–99.
31. Ghosh M, Song X, Mouneimne G, Sidani M, Lawrence DS, Condeelis JS. Cofilin promotes actin polymerization and defines the direction of cell motility. Science 2004; 304:743–6.
32. Wang W, Mouneimne G, Sidani M, et al. The activity status of cofilin is directly related to invasion, intravasation, and metastasis of mammary tumors. J Cell Biol 2006;173:395–404.
33. Koltzscher M, Neumann C, Konig S, Gerke V. Ca^{2+}-dependent binding and activation of dormant ezrin by dimeric S100P. Mol Biol Cell 2003;14:2372–84.
34. Bouwens L. Cytokeratins and cell differentiation in the pancreas. J Pathol 1998;184:234–9.
35. Bishr Omary M, Nam-On K, Liao J, Price D. Keratin modifications and solubility properties in epithelial cells and *in vitro*. In: Harris Ha, editor. Subcellular biochemistry. New York: Plenum Press; 1998. p. 105–40.
36. Wald FA, Oriolo AS, Casanova ML, Salas PJ. Intermediate filaments interact with dormant ezrin in intestinal epithelial cells. Mol Biol Cell 2005;16: 4096–107.
37. Coulombe PA, Wong P. Cytoplasmic intermediate filaments revealed as dynamic and multipurpose scaffolds. Nat Cell Biol 2004;6:699–706.
38. Izawa I, Inagaki M. Regulatory mechanisms and functions of intermediate filaments: a study using site- and phosphorylation state-specific antibodies. Cancer Sci 2006;97:167–74.
39. Masaki I, Yoichiro M, Kunio T, et al. Dynamic property of intermediate filaments: regulation by phosphorylation. Bioessays 1996;18:481–7.
40. Helfand BT, Chang L, Goldman RD. Intermediate filaments are dynamic and motile elements of cellular architecture. J Cell Sci 2004;117:133–41.
41. Hendrix MJ. Intermediate filaments. Cancer Metastasis Rev 1996;15:413–6.
42. Heizmann CW, Cox JA. New perspectives on S100 proteins: a multi-functional Ca(2+)-, Zn(2+)- and Cu(2+)-binding protein family. Biometals 1998;11: 383–97.
43. Mandinova A, Atar D, Schafer BW, Spiess M, Aebi U, Heizmann CW. Distinct subcellular localization of calcium binding S100 proteins in human smooth muscle cells and their relocation in response to rises in intracellular calcium. J Cell Sci 1998;111:2043–54.
44. Roth J, Burwinkel F, van den Bos C, Goebeler M, Vollmer E, Sorg C. MRP8 and MRP14, S-100-like proteins associated with myeloid differentiation, are translocated to plasma membrane and intermediate filaments in a calcium-dependent manner. Blood 1993; 82:1875–83.
45. Selinfreund RH, Barger SW, Welsh MJ, Van Eldik LJ. Antisense inhibition of glial S100β production results in alterations in cell morphology, cytoskeletal organization, and cell proliferation. J Cell Biol 1990;111: 2021–8.
46. Ohuchida K, Mizumoto K, Ishikawa N, et al. The role of S100A6 in pancreatic cancer development and its clinical implication as a diagnostic marker and therapeutic target. Clin Cancer Res 2005;11:7785–93.
47. Lu Z, Hu L, Evers S, Chen J, Shen Y. Differential expression profiling of human pancreatic adenocarcinoma and healthy pancreatic tissue. Proteomics 2004;4: 3975–88.
48. Shen J, Person MD, Zhu J, Abbruzzese JL, Li D. Protein expression profiles in pancreatic adenocarcinoma compared with normal pancreatic tissue and tissue affected by pancreatitis as detected by two-dimensional gel electrophoresis and mass spectrometry. Cancer Res 2004;64:9018–26.
49. Briozzo P, Morisset M, Capony F, Rougeot C, Rochefort H. *In vitro* degradation of extracellular matrix with M_r 52,000 cathepsin D secreted by breast cancer cells. Cancer Res 1988;48:3688–92.
50. Ferrandina G, Scambia G, Bardelli F, Benedetti Panici P, Mancuso S, Messori A. Relationship between cathepsin-D content and disease-free survival in node-negative breast cancer patients: a meta-analysis. Br J Cancer 1997;76:661–6.
51. Rochefort H. Cathepsin D in breast cancer: a tissue marker associated with metastasis. Eur J Cancer 1992; 28A:1780–3.
52. Cherry JP, Mordente JA, Chapman JR, et al. Analysis of cathepsin D forms and their clinical implications in human prostate cancer. J Urol 1998;160:2223–8.
53. Kristensen GB, Holm R, Abeler VM, Trope CG. Evaluation of the prognostic significance of cathepsin D, epidermal growth factor receptor, and c-erbB-2 in early cervical squamous cell carcinoma. An immunohistochemical study. Cancer 1996;78:433–40.
54. Elsasser HP, Lehr U, Agricola B, Kern HF. Establishment and characterisation of two cell lines with different grade of differentiation derived from one primary human pancreatic adenocarcinoma. Virchows Arch B Cell Pathol Incl Mol Pathol 1992;61:295–306.
55. Yamaguchi H, Pixley F, Condeelis J. Invadopodia and podosomes in tumor invasion. Eur J Cell Biol 2006;85: 213–8.
56. Weaver AM. Invadopodia: specialized cell structures for cancer invasion. Clin Exp Metastasis 2006;23:97–105.
57. Schleger C, Verbeke C, Hildenbrand R, Zentgraf H, Bleyl U. c-MYC activation in primary and metastatic ductal adenocarcinoma of the pancreas: incidence, mechanisms, and clinical significance. Mod Pathol 2002;15:462–9.
58. Fukushima N, Sato N, Prasad N, Leach SD, Hruban RH, Goggins M. Characterization of gene expression in mucinous cystic neoplasms of the pancreas using oligonucleotide microarrays. Oncogene 2004;23:9042–51.

The Role of S100P in the Invasion of Pancreatic Cancer Cells Is Mediated through Cytoskeletal Changes and Regulation of Cathepsin D

Hannah J. Whiteman, Mark E. Weeks, Sally E. Dowen, et al.

Cancer Res 2007;67:8633-8642.